Powder Technology 227 (2012) 111–122

Contents lists available at SciVerse ScienceDirect

Powder Technology

journal homepage: www.elsevier.com/locate/powtec

Numerical simulation of particle capture process of fibrous filters using Lattice Boltzmann two-phase flow model

Haoming Wang, Haibo Zhao *, Zhaoli Guo, Chuguang Zheng

State Key Laboratory of Coal Combustion, Huazhong University of Science and Technology, Wuhan 430074, People's Republic of China

ARTICLE INFO

Available online 29 December 2011

Keywords:
Lattice Boltzmann method
Filtration
Capture efficiency
Pressure drop
Fractal dimension
Porosity

ABSTRACT

The deposition of particulate matter on filter fibers (a system of cylinders) in a laminar flow normal to their axes has been simulated by a new Lattice Boltzmann model for two-phase flows. In the model, gas dynamics is solved by the Lattice Boltzmann method, while the transport of solid particle is described by the cellular automation probabilistic approach, where solid particles are constrained to move only on the same regular nodes as the fluid particles and their motion probabilities to neighboring lattices depend on the combined effect of drag forces from fluid, Brownian diffusion, and other external forces. The Lattice Boltzmann two-phase flow model is allowed to quantitatively simulate the filtration process of fibrous assembly, including the steady capture efficiency and pressure drop during the filtration processes of clean fibers, the dynamic evolution of the branch cluster structure, capture efficiency and pressure drop along with particle loading. The detailed information on the particle trajectories and the dendrite structures (fractral dimension and porosity) are obtained. Our results are in good agreement with previous theoretical predictions and experimental observations.

1. Introduction

Fiber filtration, which is at advantage of high capture efficiency of submicron particle, is very widely used for air purification in coal-fired power plants, mining engineering, cement industries, work places and life areas. Since the fifties of last century, scientists in this field have been developing mathematical models or carrying out experimental investigations to predict and improve filter performance [1–7]. However, the filtration process of suspended particles from the airflow is very complex because it involves various deposition mechanisms of solid particles (Brownian diffusion, interception, inertial impaction, and other mechanisms due to other external forces such as electrostatic force and gravity), as well as the nonsteady evolution of filtration efficiency and pressure drop during the filter clogging. These traditional methods usually obtained some empirical or semi-empirical formulations of penetration efficiency and pressure drop only [8]. In order to construct the optimal fibrous structures for high filtration efficiency (especially for particles of 0.1–1 μm), low pressure drop and long lifetime of the filter, it is essential to obtain the detailed information of a non-steady-state filtration process (e.g., the flow fields, the history of particle trajectory, the dynamic boundary due to particle deposition on the fibers, the interaction among the internal two-phase flow, the fibers and deposited particles). Numerical simulation of gas–solid two-phase flow provides a promising way to research the deposition of particulate matter on filter fibers.

Conventional numerical methods, which used Navier–Stokes equations for flow fields and Lagrangian approaches for particle motion, are usually utilized to simulate gas-particle flow in filters [9–11]. Particular difficulties arise from the non-steady-state and irregular surface caused by deposited particles. These conventional numerical methods thus have to use high-resolution and adaptive grids near the deposit and fiber, on the cost of computational efficiency and precision.

Lattice Boltzmann method (LBM) is an efficient alternative for the kind of gas–solid flows with complex and dynamic boundary conditions [12–15]. The LBM provides an approach to describe fluid phase from the perspective of mesoscopic simulation in principle [14], and it is thus capable of obtaining complex vortex structures of turbulence near fiber surfaces where particles are depositing. In the LBM, the fluid phase is considered as a large number of microscopic fictitious "fluid particles"; these fluid particles collide and migrate on the discrete lattices under regulation rules (e.g., the conversation of mass and momentum) [14]. The macroscopic characteristics of fluid motion (such as pressure, fluid density and velocity) can be obtained through statistic calculations of the fluid particles [14]. The outstanding advantages of the LBM, compared to the conventional numerical methods, include its simple and clear physical models, inherent parallelism, and capability to deal with complex and dynamic boundary conditions [14].

Basically, it is possible to distinguish gas–solid flow models based on the LBM among Lagrangian full-resolution-particle tracking

* Corresponding author. Tel.: +86 27 8754 4779x8208; fax: +86 27 8754 5526.
E-mail address: klinsmannzhb@163.com (H. Zhao).

0032-5910/$ – see front matter © 2012 Elsevier B.V. All rights reserved.
doi:10.1016/j.powtec.2011.12.057

approach, Lagrangian point-particle tracking approach, and cell automation probabilistic approach, depending on different ways for description of particle migration (Lagrangian tracking or probabilistic determination) and particle volume (full resolution or point like). As the name suggests, the Lagrangian full-resolution-particle tracking approach views solid particle as objects with geometric boundaries imposed on the fluid. The interaction between a "large" solid particle and its surrounding fluid particles is calculated by summing the transfer of momentum to the solid boundary (before and after rebound [16]) over all fluid boundary nodes [15]. The approach is capable of describing complex rheology of particle suspensions with high resolution, and then exploring complex fluid–particle interaction from the viewpoint of "true" direct numerical simulation (DNS) and providing basic parameters and even constitutive relations for macroscopic simulation. However, the approach is generally trapped into huge computational demand in cases of, for example, 10,000 particles in suspensions [15], and thus is still out of the engineering question in the foreseeable future.

With respect to the Lagrangian point-particle tracking approach (we call it the LB-Lagrangian approach in the following text), solid particle is viewed as point without volume, and the motion of each particle is directly calculated from the Lagrangian approach of the equation of motion under consideration of different external forces such as drag force, gravity, and Brownian force. The point-particle assumption is reasonable when the particles are smaller than the Kolmogorov scale of fluid phase [17]. Filippova and Hänel [18] first proposed the LB-Lagrangian approach to describe the problems of particle deposition in filters. The inertial-impaction-dominated capture efficiency from the approach agrees well with experimental results, and dendrite-like formations of particles under conditions of different Stokes numbers are captured reasonably. They [18] also noted that the interaction among changed surface and hydrodynamics and accordingly particle deposition has to be considered for the prediction of filter performance. They [18] took the view that the LB method may be the most simple and effective method to simulate gas–solid flow around such irregular and dynamic geometrical boundaries. Lantermann and Hänel [19] further proposed so-called particle Monte Carlo method to describe the trajectory of single particles by Lagrangian integration of the Langevin equation, taking into account additional forces (van der Waals forces, electrical force, …) as random forces due to Brownian movement. However, it is worth noting that the LB-Lagrangian approach may lose the parallelism (which is inherent to the LB methods) because fluid particles and solid particles were not based on the same lattices.

Another LBM-based approach for fluid–solid flows was proposed by Masselot and Chopard [12,20–22] for particle (such as snow or sand) behavior in fluid (typically, air and water). In the approach, the discrete point-like particles are constrained to exist only at the same regular lattice nodes as the fluid particles of the LBM. The state of a solid particle at a node is expressed by a Boolean variable (as those in cell automation (CA) [23] and lattice gas automation (LGA) [24]), an arbitrary number of point particles may exist at each node. During a time-step, a solid particle at a node may still stay at the original node or migrate to its nearest-neighbor node, depending on the motion probability of the particle which is determined by the combined effect of, for example, gravity, Brownian diffusion and local gas velocity. The approach is thus called cell automation probabilistic approach. Because "continuous" fluid and discrete granular media are modeled in terms of fluid particles and solid particles using the same lattices, this approach is at advantages of the convenient implementation of dynamic boundary conditions, massively parallel computation, and complicated microscopic mechanisms of solid particles (e.g., deposition, toppling, and erosion). Chopard and his colleagues used the mixed LB and CA approach (we note it LB–CA method in the following texts) to describe transport (creeping, saltation, and suspension), deposition, toppling, and erosion of snow particles in air [20], as well transport, erosion, and deposition of sands in water [12,20,21]. The ripples formed from the bottom sediments (snow or sands) and the cavity resulted from erosion around the submarine pipelines are obtained, in agreement with the real observations on the qualitative level. Gradoń and his colleagues extended the LB–CA method to describe transport, deposition, and resuspension of particular matter in fibrous filters [25,26]. The dynamic evolution of dendrite-like formations of particles on a single fiber or the composites of nano- and microsized fibers is successfully captured, and the deposition efficiency during particle loading can be calculated. Although the LB–CA method provides a way to incorporate these complex mechanisms for particle behaviors like transport, deposition and resuspension, toppling, and erosion by some simple and intuitive rules, these rules are characterized by empirical or tentative formulations/parameters. For example, an empirical constant for the ratio of particle velocity and fluid velocity is set to determine the transport probability of a particle under the action of the local fluid flow [12,20,25,26]. In the case, the influence of fluid on particle motion is described by a less rigorous or even wrong model. Although the LB–CA method can obtain some reasonable pattern of deposits through choosing appropriate characteristic parameters for particle behavior very carefully, these empirical formulations/parameters make the available LB–CA methods in open literatures be only on the level of qualitative simulation.

To sum up, the LBM-based gas–solid flow models, in comparison with conventional CFD models based on the Navier–Stokes equation for continuous fluid, have significant advantages of easily implementing complex and dynamic boundary conditions, and they are able to consider the back-influence of dynamic boundary conditions (that is, the changed surface structures due to particle deposition and resuspension, toppling, and erosion will have non-negligible effects on fluid field which influences interactively the next particle behavior). These advantages are essential for the simulation of filtration process. Among the three kinds of LBM-based gas–solid flow models, the LB–CA method is at advantages of considering complicated mechanisms of particle behavior through simple and intuitive rules, straightforward implementation of massively parallel computation [21], and less computational demand. Nevertheless, the available LB–CA methods should be improved to describe particle transport under consideration of combined effects such as Brownian diffusion, drag force, and other external forces. This paper first aims to the improvement of the existing LB–CA method in order to correctly describe particle transport among regular lattice nodes. Another aim of the paper is to simulate steady-state filtration process of clear fibers and non-steady-state filtration process during filter loading for different typical cases where either individual collection mechanism (e.g., Brownian diffusion, or interception, or inertial impaction) or simultaneous several mechanisms dominate the filtration process. It is believed that these simulations are very useful for understanding collection mechanisms and constructing optimal fibrous filter structures.

This paper is organized as follows. In Section 2.1, we introduced a standard Lattice-Boltzmann model for the carrying gas, where the so-called BGK collision rule [27,28] is used. Section 2.2 described an improved CA probabilistic approach for particle transport through correct consideration of the effect of fluid on particles. Section 2.3 shows the implementation of particle deposition and dynamic boundary conditions. In Section 3, the collection efficiencies and pressure drop of clear fibers are calculated and compared with analytical solutions or empirical formulations when one collection mechanism (Brownian diffusion, interception, or inertial impaction) is dominant. Section 4 presents the patterns of deposits and filtration characteristics of dust-loaded fibers. The fractal dimension and porosity of dendrites are investigated. Moreover, capture efficiency and pressure drop of dust-loaded fiber are also included. Finally, conclusions and outlook to future research are given in Section 5.

2. The model

2.1. The Lattice-Boltzmann model for fluid flow

Solutions of the gas flow and potential fields are first calculated using the LB method in term of Lattice Boltzmann–BGK (Bhatnagar–Gross–Krook) model [29]. In the LBM, a fictitious microscopic picture of molecular dynamics for the fluid phase is imaged, where a discrete regular grid (lattice) in space, an explicit time-steeping in time, and discrete velocities of hypothetical fluid particles are adopted. Hypothetical fluid particles are constrained to move only along the links of some regular lattices and collide at the nodes. The primary variables in the LBM, in comparison with the cellular automata and lattice-gas automata, are the so-called fluid particle density distribution function $f_i(\mathbf{x},t)$, each presenting the probable amount of fluid particles moving with a fixed velocity $\mathbf{e}_i$ along the ith direction at each node with position $\mathbf{x}$ and at discrete time t. The macroscopic hydrodynamic variables such as fluid density ρ and velocity $\mathbf{u}$ can be computed as the first two moments of f_i:

$$\rho = \sum_{i=0}^{Q-1} f_i,\ \rho u = \sum_{i=0}^{Q-1} f_i e_i \tag{1}$$

where Q is the number of discrete velocities, depending on the lattice topology. In the present paper, a filtration process of a row of cylindrical fibers in a laminar flow normal to their axes is considered, which can be viewed to be two-dimensional gas–solid flows. Our LBM implementation uses the D2Q9 model [27] with nine velocities in a two-dimensional domain with the same sampling Δx in both x- and y-directions (shown in Fig. 1).

The evolution of the density distribution functions at each time step is given by the discretized BGK model [27]:

$$f_i(\mathbf{x}+\mathbf{e}_i\Delta t, t+\Delta t) - f_i(\mathbf{x},t) = \left[f_i^{eq}(\mathbf{x},t) - f_i(\mathbf{x},t)\right]/\tau \tag{2}$$

where τ is a dimensionless parameter termed the relaxation time; $\mathbf{x}+\mathbf{e}_i\Delta t$ is a nearest node of the node with position $\mathbf{x}$ along the direction i; each distribution function f_i corresponds to a certain velocity vector $\mathbf{e}_i$ (here $i=0,\ldots,8$); and f_i^{eq} is the equilibrium distribution function defined as [27]:

$$f_i^{eq} = \rho\alpha_i\left[1 + \frac{\mathbf{e}_i\cdot\mathbf{u}}{c_s^2} + \frac{1}{2}\left(\frac{\mathbf{e}_i\cdot\mathbf{u}}{c_s^2}\right)^2 - \frac{\mathbf{u}^2}{2c_s^2}\right] \tag{3}$$

in which α_i is the fixed weighting coefficient, dependent on the length of the corresponding lattice vector. In the D2Q9 model [27], $\alpha_0 = 4/9$, $\alpha_i = 1/9 (i=1,3,5,7)$, $\alpha_i = 1/36 (i=2,4,6,8)$; c_s is the local speed of sound of the chosen LBM model, and for D2Q9 it is $c_s = c/\sqrt{3}$ with $c = \Delta x/\Delta t$.

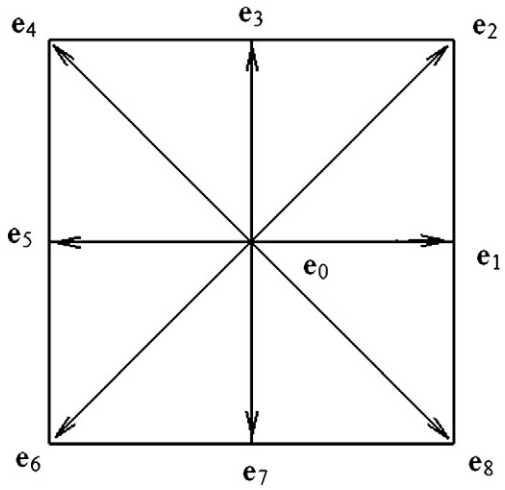

Fig. 1. Discrete velocities in D2Q9 model.

In fact, the LB Eq. (2) consists of two steps: a collision step and a streaming step. The right and left sides of Eq. (2)correspond to the collision and streaming step, respectively. Eq. (2) implies that the difference of the original $f_i(\mathbf{x},t)$ and the streamed $f_i(\mathbf{x}+\mathbf{e}_i\Delta t, t+\Delta t)$ is related to the changes due to collisions during the motion of the fluid particles, and the collisions redistribute the distribution function toward equilibrium state f_i^{eq} with change a rate of $1/\tau$. By performing the streaming step and the collision step successively at each grid point, the LBM algorithm proceeds. The fluid pressure field P is determined by the equation of state for a discrete space:

$$P = \rho {c_s}^2 \tag{4}$$

The LBM represents a first-order explicit finite-difference discretization of the finite discrete velocity model of the Boltzmann equation [14]. It is well known from the kinetic theory of gasses that the Navier–Stokes equations usually used in macroscopic simulation are solutions of the Boltzmann equation in the continuum regime [30]. Consequently, Eq. (2) can correctly reproduce the incompressible Navier–Stokes equations with second-order accuracy in space, giving the speed of sound c_s and the kinematic viscosity of the fluid

$$\upsilon = \frac{c_s^2}{2}(2\tau - 1). \tag{5}$$

It is worth noting that the filtration process is a case of the dilute gas–solid flows and the effect of particles on the fluid (the gas phase modification due to the presence of particles) is thus neglected. In fact, the so-called two-way coupling effect can be considered through an additional force (which represents the reacting drag force and describes the interaction between the fluid and particle phases) in the LB evolution Eq. (2)[14,31]. Furthermore, high Reynolds number flows can be simulated by the LBM by introducing the so-called Smagorinsky subgrid model to increase locally the relaxation time [32].

2.2. The cell automation probabilistic model for particle transport

Particle transport in fluids depends on the combined effects of the fluid–particle interaction, gravity and buoyancy, and even Brownian diffusion and electrostatic force. Masselot and Chopard [20,21] first proposed the CA probabilistic model to describe particle transport, where solid particles are constrained to only move on the same regular lattices as the fluid particles, and their transport probabilities to neighboring nodes depend on the local fluid flow and other external forces subject to solid particles. Let $N(\mathbf{x}_p,t)$ be the number of simulation particles at site $\mathbf{x}_p$ and time t. $N(\mathbf{x}_p,t)$ can take any nonnegative value. The key idea of the CA probabilities model is that each of the $N(\mathbf{x},t)$ particles jumps to a neighboring node at site $\mathbf{x}_p+\mathbf{e}_i\Delta t$ with a probability p_i proportional to the projection of the actual displacement of the particle in the direction $\mathbf{e}_i$. Fig. 2 illustrates an example of the transport rule for the D2Q9 model. Let a particle locate at site $\mathbf{x}_p$ and time t. After a time-step Δt its new position $(\mathbf{x}_p{}^*)$ is $\mathbf{x}_p+\mathbf{u}_p\Delta t$, where $\mathbf{u}_p$ is the particle velocity at time t. It is noted that the time-step is constrained to be less than the crossing time scale of solid particle to the grid, in such a way that a solid particle moves to its nearest-neighbor node within Δt at maximum. Usually the new position does not coincide with any node of the grid. The transport probabilities of the particle awards to the east, north, west, and south direction, i.e., p_1, p_3, p_5 and p_7, are calculated in the D2Q9 model:

$$p_i = \max\left(0, \left(\mathbf{u}_p\cdot\mathbf{e}_i\right)\frac{\Delta t}{\Delta x}\right) = \max\left(0, \frac{\Delta x_p}{\Delta x}\cdot\mathbf{e}_i\right), i = 1,3,5,7 \tag{6}$$

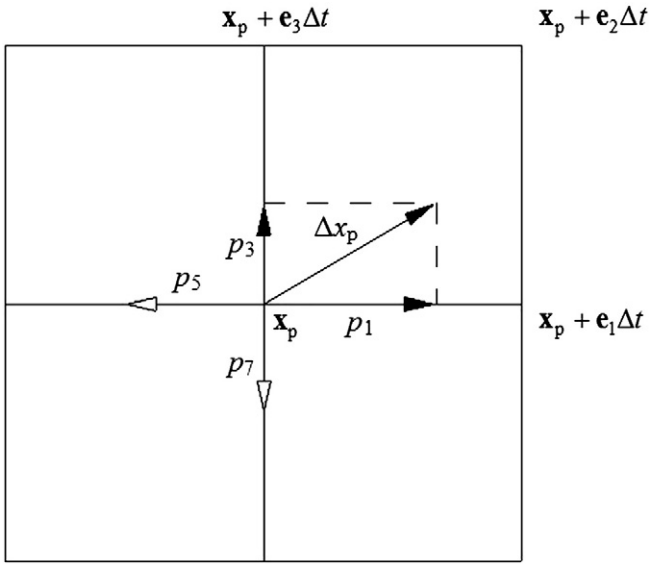

Fig. 2. Particle transport rule in the CA probabilistic model.

where Δx_p is the actual displacement of the particle within time step Δt, $\Delta x_p = \mathbf{x}_p^* - \mathbf{x}_p = \mathbf{u}_p \Delta t$. It is clear that $p_i \times p_{i+4} = 0$ since $\mathbf{e}_i = -\mathbf{e}_{i+4}$.

The solid particle may still stay at the original node or jump to a nearest-neighbor node, depending on the transport probabilities to directions 1, 3, 5 and 7:

$$\mathbf{x}_p^* = \mathbf{x}_p + \mu_1\mathbf{e}_1 + \mu_3\mathbf{e}_3 + \mu_5\mathbf{e}_5 + \mu_7\mathbf{e}_7 \tag{7}$$

where μ_i is a Boolean variable which is equal to 1 with probability p_i. Giving a typical example as shown in Fig. 2, where $p_1 > 0$, $p_3 > 0$, $p_5 = 0$, and $p_7 = 0$. It means the particle may stay at rest with probability $(1-p_1)(1-p_3)$, or jumps to east with probability $p_1(1-p_3)$, to north with probability $p_3(1-p_1)$, to north-east with probability $p_1 p_3$. As for numerical implementation, two independent random numbers from a uniform distribution in the interval [0,1], r_1 and r_2, are first generated through random number generator. The following conditions are used to determine the new position of the particle by Monte Carlo method:

$$\begin{cases} \text{if } r_1 > p_1 \text{ and } r_2 > p_3, \mathbf{x}_p^* = \mathbf{x}_p \\ \text{if } r_1 < p_1 \text{ and } r_2 > p_3, \mathbf{x}_p^* = \mathbf{x}_p + \mathbf{e}_1\Delta t \\ \text{if } r_1 > p_1 \text{ and } r_2 < p_3, \mathbf{x}_p^* = \mathbf{x}_p + \mathbf{e}_3\Delta t \\ \text{if } r_1 < p_1 \text{ and } r_2 < p_3, \mathbf{x}_p^* = \mathbf{x}_p + \mathbf{e}_2\Delta t \end{cases} \tag{8}$$

It is proven that the binomial scattering can be approximated by a Gaussian distribution if the number of simulation particles is large enough [33].

Unfortunately, the existing CA probabilistic model only estimates roughly the actual displacement of a particle within a time step. For example, the displacement of sand/snow particle under the action of the local fluid flow and gravity force is $\Delta t_s \mathbf{w}$ in the original model proposed by Masselot and Chopard [20], where Δt_s is the time-step associated to solid particle motion, $\mathbf{w}$ is velocity of solid particle, $\mathbf{w} = \mathbf{u} + \mathbf{u}_{fall}$, with $\mathbf{u}$ the local fluid velocity and $\mathbf{u}_{fall}$ the falling velocity (accounting for gravity force). The ratio $\Delta t_s/\Delta t$ is set as an empirical constant to describe the effect of fluid on particle motion indirectly and qualitatively. The transport probability is thus calculated as follows [20]: $p_i = \max(0, (\Delta t_s/\Delta x)(\mathbf{e}_i \cdot \mathbf{w})) = \max(0, (\Delta t_s/\Delta t)(\mathbf{e}_i \cdot \mathbf{w})/|\mathbf{e}_i|^2)$. Usually $\Delta t_s \geq \Delta t$ for efficiency, but small enough to ensure p_i is always less than 1. Obviously, particle velocity and displacement here are not accurate and even not of the correct order of magnitude. We improve the original model by quantitatively calculating the velocity and displacement of solid particles under the combined effect of, for example, drag force from local fluid and Brownian diffusion, which is necessary for the filtration processes.

Brownian diffusion has significant effect on the motion of, especially, small particles. It is well-known that the collection of submicron particles by fibrous filters is dominated by the mechanism of Brownian diffusion. Particle movement in the space due to Brownian diffusion can be regarded as certain random walk process, where the transition probability (which depends on diffusion coefficient (D) and is a function of particle diameter, medium temperature and surrounding flow velocity from the theoretical Stokes–Einstein equation) is calculated to determine quantitatively the random movement of particles. The transition probability, which is characterized by multiple integration, is usually complicated and time-consuming in calculation [34]. Przekop et al. [25] introduced another stochastic method to consider random (diffusional) displacement of the solid particles in the CA probabilistic model, where the frequency, k_0, of the particle jump between the neighboring lattices are determined by diffusion coefficient D and the lattice length Δx, i.e., $k_0 = D/\Delta x^2$. They chose a constant k_0 from a specified Peclet number dependent on cases. The constant k_0 may diverge from real situations. Brownian dynamic simulation is also able to depict the random behavior of particles [35]. On the other hand, it is feasible to introduce Brownian force [36] or Brownian acceleration [37] in the Lagrangian equations of motion for a particle to take Brownian diffusion into account. Lantermann and Hänel [19] introduced a time-dependent stochastic acceleration term in the Langevin equation to represent the Brownian motion of small particles. Kim [36] investigated particle behavior in membrane system by taking drag force, Brownian force, and electrostatic repulsion into account. In this paper, random Brownian force [36,38] is introduced to consider the Brownian diffusion. The particle motion is thus described by the Newtonian equation under consideration of drag force $\mathbf{F}_D$ and Brownian force $\mathbf{F}_B$ [9–11]:

$$\frac{d\mathbf{u}_p}{dt} = \mathbf{F}_D + \mathbf{F}_B = \frac{\mathbf{u} - \mathbf{u}_p}{\tau_p} + \varsigma\sqrt{\frac{216\mu k_B T}{\pi\rho_p^2 d_p^5 \Delta t}} \tag{9}$$

$$\frac{d\mathbf{x}_p}{dt} = \mathbf{u}_p \tag{10}$$

where τ_p is the relaxation time scale of particle, $\tau_p = \rho_p d_p^2 C_c/(18\,\mu)$; μ is the dynamic viscosity of gas; d_p and ρ_p are particle diameter and density respectively; C_c is an empirical correction factor called Cunningham slip correction factor, here $C_c = 1$ for simplicity; ς is zero-mean, unit-variance independent Gaussian random number; k_B is Boltzmann constant; T is gas temperature.

In the Lagrangian particle tracking approaches, particle velocity and position are calculated by integration of the equations of motion for the particle. In this paper, in order to save computational time, the particle velocity and displacement can be explicitly calculated through integration of the equations of motions over time t successively:

$$\mathbf{u}_p^* = \mathbf{u}_p \cdot \exp\left(-\frac{\Delta t}{\tau_p}\right) + \left(\mathbf{u} + \mathbf{F}_B \cdot \tau_p\right) \cdot \left(1 - \exp\left(-\frac{\Delta t}{\tau_p}\right)\right) \tag{11}$$

$$\mathbf{x}_p^* = \mathbf{x}_p + \left(\mathbf{u}_p - \mathbf{u}\right)\left(1 - \exp\left(-\frac{\Delta t}{\tau_p}\right)\right) + \mathbf{u}\Delta t + \left(\Delta t + \left(1 - \exp\left(-\frac{\Delta t}{\tau_p}\right)\right) \cdot \tau_p\right) \cdot \mathbf{F}_B \cdot \tau_p \tag{12}$$

The accurate particle displacement $\Delta x_p (= \mathbf{x}_p^* - \mathbf{x}_p)$ within the period Δt is thus obtained. As a result, the transport probabilities of the particle can be calculated quantitatively through Eq. (6).

The present CA probabilistic model is able to consider particle transport under the action of other external forces such as gravitational

force and buoyancy, electrical forces and van der Waals forces, by adding these forces into Eq. (9). It is also possible to take into account particle rotation by angular velocity of particles, if necessary.

Once the particle position and velocity are determined by the model, the particle fields can be obtained by statistics of all simulation particles over all nodes. Simulation particles are usually weighted to represent these real particles. That is, the number, $N_r(\mathbf{x},t)$, of real particles at site $\mathbf{x}$ and time t can be calculated by: $N_r(\mathbf{x},t)=\sum_{i=1}^{N(\mathbf{x},t)} w_i$; the velocity, $\mathbf{u}_p(\mathbf{x},t)$, of real particles is given by $\mathbf{u}_p(\mathbf{x},t)=\sum_{i=1}^{N(\mathbf{x},t)} w_i\mathbf{u}_{p,i}$; and other variables of particle fields can be calculated using the similar ways, where w_i and $\mathbf{u}_{p,i}$ are the weight and velocity of the i-th simulation particle at site $\mathbf{x}$ and time t.

2.3. Dynamic boundary

As the particles deposited, the shape of fiber surface continues to change, resulting in some dendrite-like clusters consisting of deposited particles. Both fiber and clusters serve as collectors of the coming particles. Furthermore, the dynamic evolution of dendrites affects the flow fields and thus the subsequent particle deposition. It is necessary to consider the interaction between two-phase flow fields and non-steady surface geometry. In the LB methods, the complex boundary conditions can be dealt with very simple rules.

There are three kinds of nodes in LBM-based two-phase models: fluid node, solid node and boundary node. Fluid particles and solid particles within fluid nodes can evolve according to Eqs. (2) and (6), respectively. Solid nodes are occupied by rigid wall (here fibers) or deposited particles, and it is impossible that fluid particles and solid particles enter into solid nodes. As suggested by Chopard et al. [22], up to N_{thres} solid particles can accumulate on a solid node (the value of N_{thres} depends on diameter of solid particles, lattice length Δx and real size of computational domain). If the number, N_{depo}, of deposited particles in a node is less than N_{thres}, the node is viewed as boundary node. In a boundary node, solid particles are limited to rest, and fluid particles are not affected by the presence of these solid particles. It is assumed that any particle is stopped and deposited once it contacts fiber surface or a previously deposited particle (that is, if its next position is a solid node or a boundary node). If the next position is a solid node, the current node of the particle will become a boundary node from a fluid node, and $N_{depo}=1$. If the next position is a boundary node, $N^*_{depo}=N_{depo}+1$. Once N^*_{depo} is equal to a specified N_{thres}, the node is altered from "boundary node" to "solid node". The solidification process implies a dynamically changing boundary condition for the two-phase flows.

Fluid particles within fluid nodes or boundary nodes may collide with rigid obstacles or walls which are represented by solid nodes. Bounce-back boundary condition (bbc) with second-order accuracy is adopted, saying, fluid particles bounce back from where they came (as shown in Fig. 3). The bbc expression is given by:

$$f_{-i}(x_0,t)=f_i(x_0,t) \tag{13}$$

3. Capture efficiency and pressure drop of clean fibers

3.1. Flow field

The two-dimensional computational domain is a square with side length of h, and a cylinder with diameter d_f representing the fiber is placed in the regional center, $d_f/h=1/4$, as shown in Fig. 4. The direction of flow carrying particles is perpendicular to the cylinder axis. Upper and lower boundaries are considered to be periodic, that is, a fluid particle or a solid particle moving out the domain from the upper or lower boundary will enter into the domain from the opposite boundary at once. The evolution of distribution function under the periodic boundary conditions is given by:

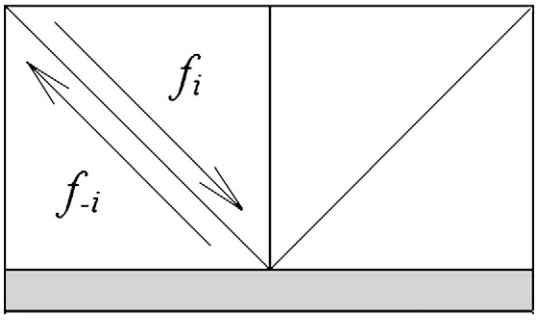

Fig. 3. Bounce-back boundary condition in the LB method.

$$f_i(0,t+\Delta t)=f_i'(h,t),\qquad f_i(h,t+\Delta t)=f_i'(0,t) \tag{14}$$

where superscript "′" represents distribution function after colliding. In such a way, a system of parallel cylinders in a flow normal to their axis is considered. 256×256 nodes are chosen to represent the computational domain, and the grid resolution is proved to be good enough to obtain reliable flow fields.

The inlet velocity of fluid is constant: $u(y)=u_0$, and it is considered that the initial velocity of solid particles in the inlet is same to the fluid velocity. In the outlet, the flow field is regarded as fully developed, i.e., $\partial u/\partial x=\partial v/\partial x=0$. Non-equilibrium extrapolation scheme is used here to deal with inlet and outlet boundary conditions [39]. The basic idea is to decompose the distribution function at the boundary node into its equilibrium and non-equilibrium parts and then to approximate the non-equilibrium part with a first-order extrapolation of the non-equilibrium part of the distribution at the neighboring fluid node [40]:

$$f_i(\mathbf{x}_b)=f_i^{eq}(\mathbf{x}_b)+\left[f_i(\mathbf{x}_f)-f_i^{eq}(\mathbf{x}_f)\right] \tag{15}$$

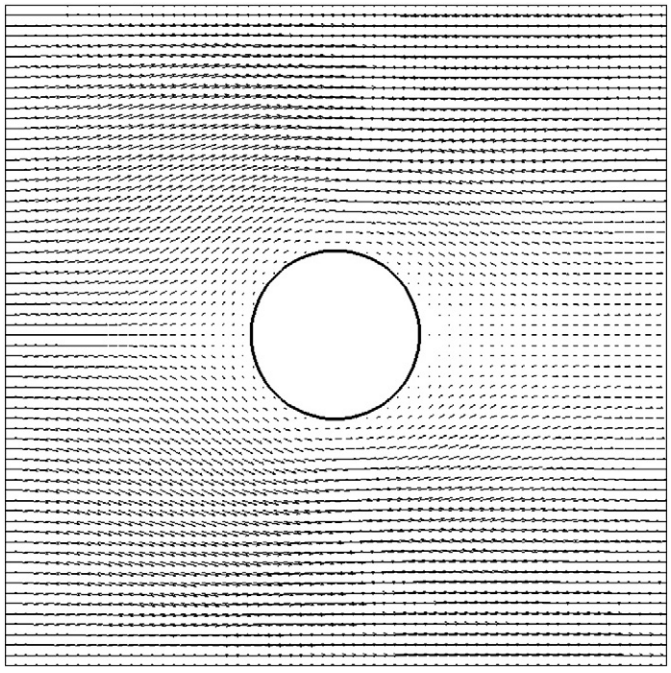

Fig. 4. Velocity vector of flow field.

where $\mathbf{x}_f$ is the nearest neighbor fluid node of boundary node $\mathbf{x}_b(\mathbf{x}_f = \mathbf{x}_b + \mathbf{e}_i\Delta t)$.

Eq. (16) presents the error of simulation results. The flow field is considered as stable when error $<10^{-5}$.

$$\text{error} = \frac{\sum_{j,i} \left|u^*_{j,i} - u_{j,i}\right|}{\sum_{j,i} \left|u^*_{j,i}\right|} \tag{16}$$

where $u_{j,i}$ is the fluid velocity of a node indexed by j in y dimension and i in x dimension. Once the flow field reaches stable state (a steady-state velocity distribution is shown in Fig. 4), solid particles with a low volume fraction of 0.01 are injected from the entrance. The initial node of a solid particle is random.

The capture efficiency and pressure drop of loaded filters are related to not only the loaded mass but also the performance of clear fibers. We first simulated particle capture process of clear fibrous filters using the LB–CA method in the section. In the following cases, particles will "disappear" if they deposited on fibers, so the shape of fiber does not change and the fiber keeps "clean".

3.2. Capture efficiency of clean fiber

Fiber capture efficiency can be calculated as follows:

$$\eta = \frac{G_1 - G_2}{G_1} \times 100\% \tag{17}$$

where G_1 is the total number of solid particles entering the computational domain from the inlet per unit time (monodisperse particles are considered in this paper); G_2 is the total number of particles leaving the computational domain from the outlet per unit time.

Three main mechanisms for particle collection by fibers are considered: Brownian diffusion, interception, and inertial impaction. It is well known that the capture efficiency due to Brownian diffusion is related to Peclet number Pe, $Pe = Ud_f/D$, where D is the Brownian diffusion coefficient, $D = k_BT/(3\pi\mu d_p)$; U *is* average velocity for the stream; d_f is the fiber diameter; The interception efficiency depends on fiber structure which is characterized by the ratio of particle size and fiber equivalent diameter, namely the intercept coefficient $R = d_p/d_f$; Stokes number ($St = \rho_p d_p^2 U/(18\mu d_f)$, where ρ_p is the particle density) has crucial effects on inertial-impaction-dominated collection efficiency. Generally speaking, fibrous filter has high capture efficiencies for large particles (generally larger than 10 μm with large St number, and the inertial impaction mechanism dominates) and small particles (generally less than 0.01 μm with large D and small Pe number, and the Brownian diffusion mechanism dominates). However, intermediate particles (especially fine particles in range of 0.1–1 μm, who are situated in "Greenfield gap" range [41]) are hardly captured by the fibers because the two important collection mechanisms, Brownian diffusion and inertial impaction, have the minimum effect on those particles and the contribution of interception mechanism on capture efficiency is also weak. By adjusting the three dimensionless numbers (Pe, R, and St), we can study the fiber capture efficiency when an individual capture mechanism is dominant. The numerical results of the LB–CA model can be quantitatively compared with these of the existing empirical/semi-empirical/analytical formulas.

We first simulated the Brownian-diffusion-dominated collection processes, where particle size is comparatively small and R is set as 1/64. Dimensional analysis of external forces acting on particles shows that the Brownian force is much larger than the drag force. Random Brownian diffusion of particles is much stronger than the convection diffusion. The trajectories of particles are relatively chaotic, and some of the particles can even randomly move to the leeward of the fiber and deposit after colliding and contacting with the fiber (Fig. 5). The capture efficiency from the numerical simulation agrees

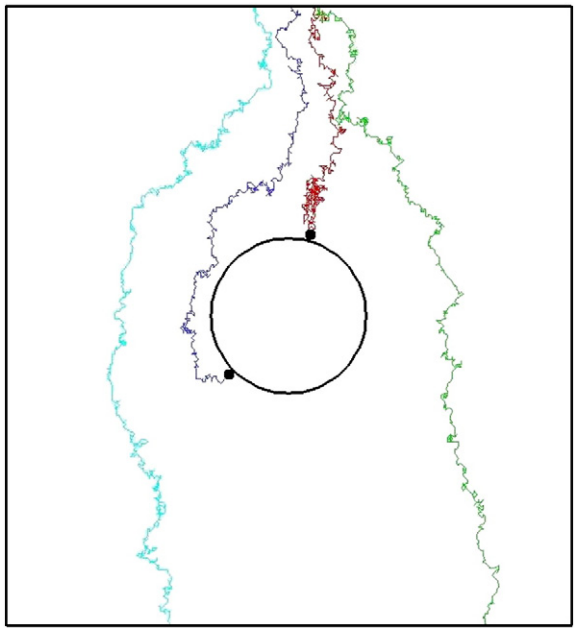

Fig. 5. Typical particle trajectories in Brownian-diffusion-dominated cases.

well with these predictions by some existing theoretical formulas (Stechkina and Fuchs [42], Lee and Liu [43]), as shown in Fig. 6a. When Pe number ranges from 1000 to 10000, the results are all

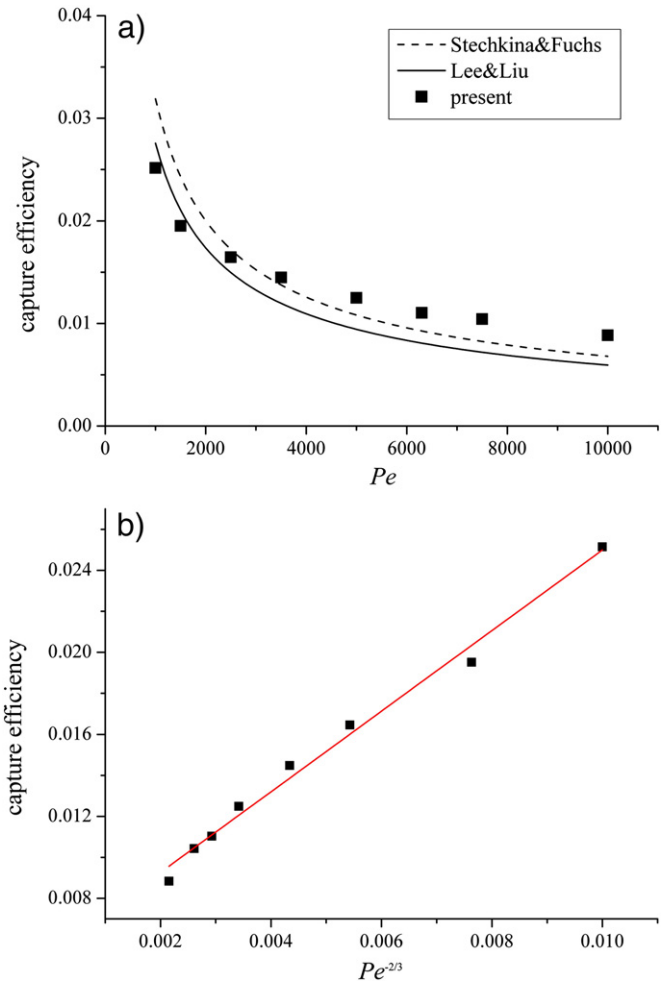

Fig. 6. Capture efficiency in Brownian-diffusion-dominated cases: (a) vs Pe; (b) vs $Pe^{-2/3}$.

within two analytical solutions, although there is a certain deviation with any theoretical prediction. It is found that when *Pe* number is comparatively smaller (from 1000 to 5000, where it is deduced that the contribution of Brownian diffusion mechanism on capture efficiency is comparatively stronger), the simulation results fit the two formulas better, and for larger *Pe* number (within the range of 5000 to 10,000) the numerical results are slightly higher than theoretical predictions. In fact, although the Brownian diffusion mechanism dominates under the condition, the drag force of fluid on the particles is still considered in the simulation (namely, particles still have a small inertia), especially when *Pe* is large ($5000<Pe<10{,}000$). That is, the obtained capture efficiency is actually the overall efficiency of the three capture mechanisms considered, while the theoretical formulas only consider the capture efficiency from Brownian diffusion. It is noted that the capture efficiency dominated by the Brownian diffusion mechanism is proportional to $Pe^{-2/3}$ (see Fig. 6b) in general, which is consistent with the classical theory [42].

For larger particles, *St* is larger. Dimensional analysis shows that the Brownian force on a particle is far less than the drag force from the fluid. The particle trajectory at initial stage is nearly consistent with the fluid path. However, as particles are approaching the fiber, particles apparently deviate from the path of the fluid because of their own larger inertia, resulting in particles' head-on impaction on the windward of fiber (see Fig. 8). In these cases inertial impaction mechanism dominates, the relationship between capture efficiency and *St* number is presented in Fig. 7. The agreement between the numerical results and Brown's empirical formula (for low *St* condition) [44] is good. When *St* number becomes larger, the capture efficiency are also increasing. It is shown in Fig. 7 that the obtained capture efficiency deviates slightly from the existing prediction when $St=0.05$, 0.1, 0.2. This is because the inertia of particles with low *St* is not intense enough and the particles still follow the trajectories of fluid particles to a certain extent. Therefore, interception mechanism plays some roles in this condition. When *St* number continuously increases, the dominant role of inertial impaction mechanism becomes stronger and stronger.

Interception mechanism affects the capture process of particles of all sizes, however the contribution on the overall capture efficiency is comparatively little in general. With respect to intermediate particles, the Brownian diffusion is relatively weak, and their inertia is also relatively low. Therefore, the interception mechanism is highlighted to be the most important collection mechanism. In these cases, the particle trajectories in the whole flow field basically correspond to the fluid streamlines (see Fig. 10). When the particles move close to the fiber, the particles may impact the fiber and be intercepted if the distance between particle centroid and fiber wall is less than or equal to

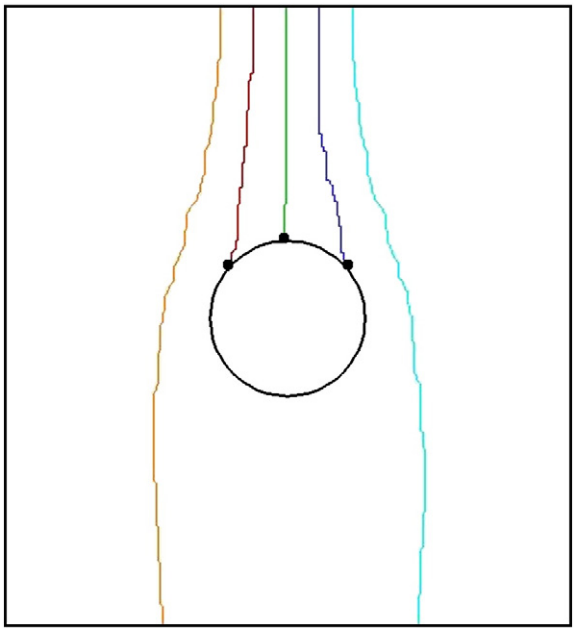

Fig. 8. Typical particle trajectories in inertial-impaction-dominated cases.

the particle radius. In these simulations, the fiber diameter is adjustable and the particle diameter is fixed, in such a way that the variable *R* is obtained to study the relationship between *R* and the capture efficiency. As shown in Fig. 9, the simulation results correspond with these existing theoretical formulas of Lee and Liu [45] and Lee and Gieseke [46] very well.

3.3. System pressure drop

Pressure drop ΔP across a filter is another important parameter of fiber filters. It depends on the thickness d_f of the filter, the air viscosity μ, the incoming flow velocity U, the fiber volume fraction α, and other variables. Pressure drop ΔP can be related to drag force F_D on a unit length of a single fiber oriented transverse to the flow as [8]: $\Delta P=F_D d_f/A$, where A is the cross-sectional area, $A=h^2$. Dimensionless drag force F^* is defined as: $F^*=F_D/(\mu U)$.

When the Reynolds number $Re(=Ud_f/\nu)$ is less than 1.0, the system pressure drop are nearly constant and independent of the Reynolds number [8]. It is mainly related to the volume fraction of fiber. In our simulation, the fiber diameter is small enough and $Re=0.2$. There are two theoretical formulas to describe the

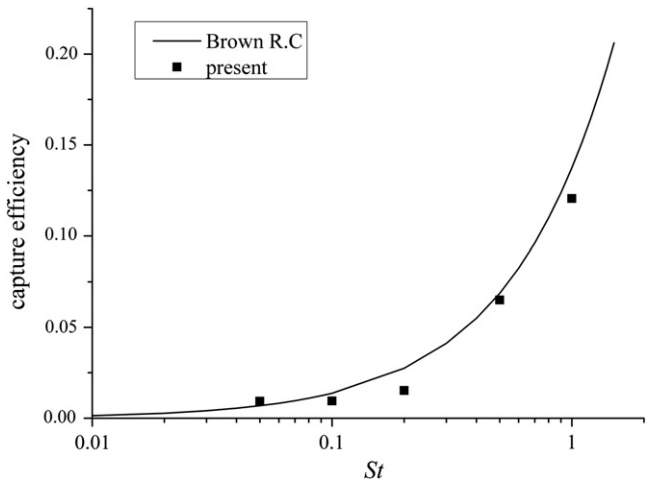

Fig. 7. Capture efficiency in inertial-impaction-dominated cases.

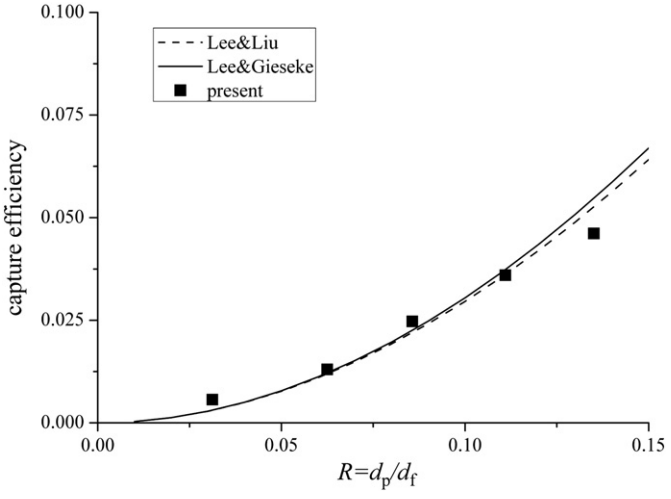

Fig. 9. Capture efficiency in interception-dominated cases.

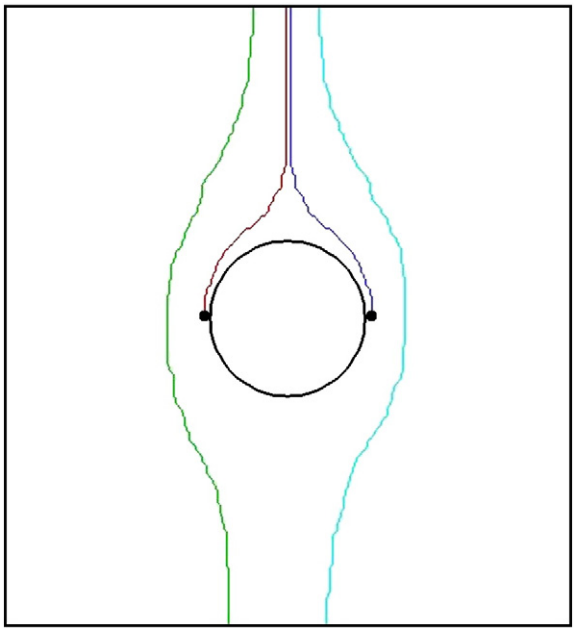

Fig. 10. Typical particle trajectories in interception-dominated cases.

relationship between the dimensionless drag force and fiber volume fraction α.

Miyagi's formula for an isolated row of parallel fibers is [47]:

$$F^* = 4\pi\left[-\ln\frac{d_f}{2h} - 1.33 + \frac{\pi^2}{3}\left(\frac{d_f}{2h}\right)^2\right]^{-1} \tag{18}$$

Kuwabara's Formula is expressed as [8]:

$$F^* = 4\pi\left[-0.5\ln\alpha - 0.75 - 0.25\alpha^2 + \alpha\right]^{-1} \tag{19}$$

where the fiber volume fraction $\alpha = \pi d_f^2/(4\,h^2)$.

We obtained dimensionless drag forces over five fiber volume fractions by changing the fiber diameter. F^* increases as α increases, which is very close to the predicted results of the two expressions, shown in Fig. 11.

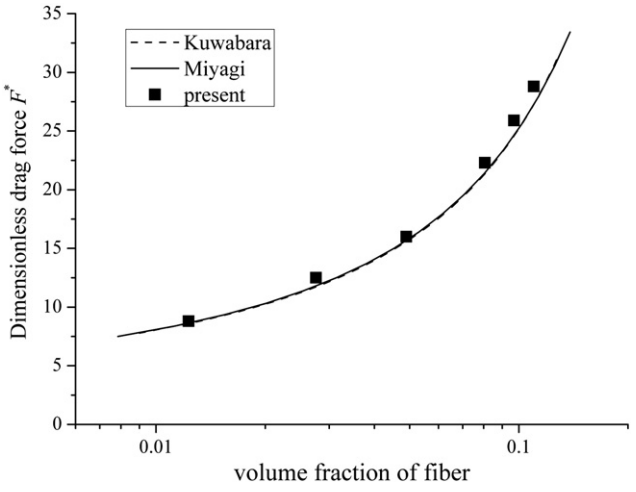

Fig. 11. Relationship between dimensionless drag force and filter volume fraction.

4. Dynamic evolution in capture process

In real cases, particles will deposit on the surface of the fiber, which will change the shape of fiber and thus affect the flow field. On the other hand, the formed dendrite-like clusters will have significant effect on capture efficiency and pressure drop. It is necessary to investigate the dynamic formation of dendrite-like clusters. In the following simulations, flow fields and particle fields are both calculated in each time step in order to capture the characteristics of the non-steady processes. Several important parameters, fractal dimension, porosity, capture efficiency, and pressure drop, of the dust-loaded fibers are calculated.

4.1. Dynamic evolution of deposition patterns dominated by individual capture mechanism

Kanaoka et al. [48] presented the relationship between deposition patterns and filtration condition (in terms of the non-dimensional filtration parameters Peclet number *Pe* and Stokes number *St*) by Monte Carlo simulation for the growing processes of particle dendrites on a fiber in Kuwabara's cell. The three extreme conditions, $Pe = 0$, $Pe = \infty$ and $St = 0$, $St = \infty$, are capable of representing predominant Brownian diffusion, interception and inertial impaction, respectively [49]. Pure Brownian diffusion leads to an isotropic distribution of particles around the fiber with relatively open pore structure, and the interception mechanism results in two striking dendrites located on 45° and 135° of cylinder surface and growing up along the opposite direction of flow steam, and the inertial collision mechanism makes the particles deposit on the windward of fiber. These deposition patterns have been observed experimentally. The LB–CA model provides the detailed knowledge on the dynamic evolution of dendrites, as shown in Fig. 12. Fairly good agreement in shape of dendrites is obtained with reference results. The LB–CA model is able to capture the non-steady-state filtration process correctly.

Factually, when Brownian diffusion is dominant (that is, *Pe* is very small) the Brownian force F_B is far larger than the drag force (Eq. 9), resulting in a very stochastic trajectory of particles (see Fig. 13(a)). Particles deposited at any position of surface around the fiber. Later on, particle deposition occurs on the existing dendrites around the fiber, leading to an isotropic distribution of particles around the fiber with relatively open pore structure. If *Pe* becomes very large and *St* is very small, Brownian force of particles is negligible and particles fully follow the steamline of fluid (Fig. 13(b)), resulting in particle deposition in two special positions of windward cylinder (located on 45° and 135° of cylinder surface) and growing up along the opposite direction of flow stream. It is obvious that the dendrites are able to capture the incoming particles. It is noted that some particles deposited on the leeward due to Brownian diffusion (in this case, $Pe = \infty$ and $St = 2.7\times10^{-6}$). With regard to predominant dominant inertial impaction mechanism, very large *St* means particles have very large inertia and cannot deviate from their original direction, leading to compact structures facing the flow (see Fig. 13(c)). It is noted that the trajectories of particles, and factually, fluid streamlines are different from these shown in Figs. 5, 8 and 10, which correspond to the filtration processes of clean fibers. It is because the formed dendrites influence the flow fields and then the particle trajectories.

4.2. Fractal dimension of dendrites by various capture mechanisms

Fractal dimension (D_f) is introduced to investigate the growth of dendrites. Fractal dimension can measure irregularity of complex objects, and it can reflect the effectiveness of space possession. Box counting method is used here to calculate fractal dimension of dendrites during the clogging processes.

As shown in Fig. 14, during the early stage of dendrite formation (the number of deposited particles is less than 400), fractal dimensions

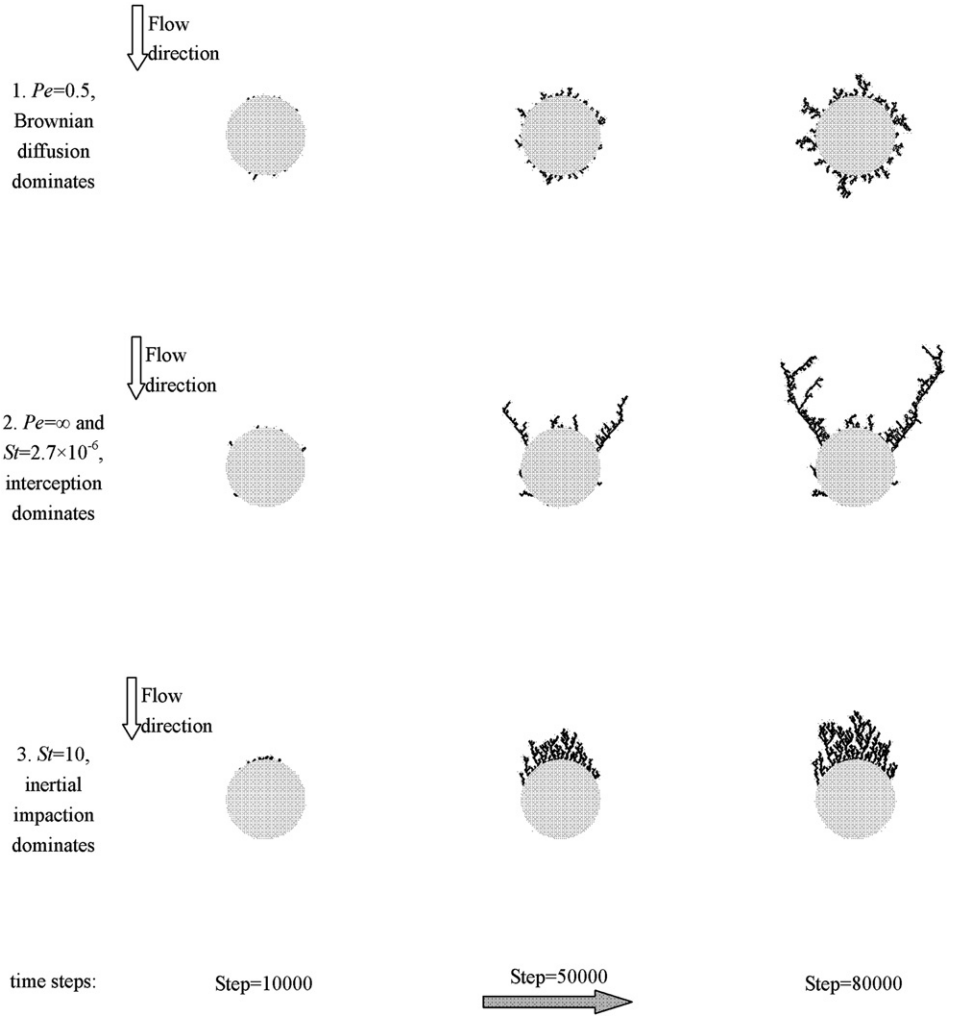

Fig. 12. Dynamic evolution of deposition patterns by the LB–CA model.

dominated by different capture mechanisms are almost same, increasing from 1 to 1.25 for the 2-dimensional cases. Then, different trends occur because of various deposition patterns. With respect to predominant Brownian diffusion mechanism, D_f increases continuously, almost showing a linear growth trend. This is because particles could deposit in any position around the fiber and then occupy the space more effectively. Under the predominant role of interception mechanism, D_f keeps nearly invariant or slightly reduces when the number of deposited particles is 400–500; then $D_f$increases linearly. This is because the dendrites mainly grow along their longitudinal direction at 45° and 135° of cylinder surface during the period of 400–500 deposited particles; then, the particles begin to deposit on the front of two main dendrites, resulting in the linear increasing of D_f. When inertial collision mechanism dominates, D_f fluctuates around 1.35 along with the capture process, which illuminates that the irregularity of dendrites does not change any more.

4.3. Porosity of dendrites by various capture mechanisms

Porosity is another characteristic of dendrites. The average porosity is usually defined as following:

$$\varepsilon = 1 - \sum_{i=1}^{n} V_i \Big/ V \tag{20}$$

where V_i is the volume of the i-th particles, V is the total volume of dendrites, n is the number of deposited particles. Usually, the porosity is obviously different in the radial direction. In this paper the distribution of porosity over different particle layer is obtained. Particles are sphere and monodisperse, so the dendrites can be divided into many layers, as shown in Fig. 15. Porosity of i-th layer can be expressed as:

$$\varepsilon_i = 1 - \frac{n_i \cdot V_{\mathrm{p}}}{V_{lay,i}} \tag{21}$$

where n_i is particle number within i-th layer, V_{p} is the volume of particle and $V_{lay,i}$ is the total volume of the i-th layer.

Fig. 16 presents the porosity distribution of dendrites when individual capture mechanism is dominated. Generally speaking, the porosity is lower at lower layer and higher at upper layer; the porosity first decreases then increases and finally approaches to steady along the increasing of particle layers; the porosity of the first layer is usually higher than that of other layers, except the case of predominant Brownian diffusion; below the fifteenth layer the Brownian-diffusion-dominated porosities are less, and the porosities in predominantly inertial impaction mechanism are larger than the other two at the late stage (above the 15th layer). These observations are reasonable throughout understanding the nature of different capture mechanisms and considering the famous "shielding" effect of the previously deposited particles. The results presented in Figs. 12–14, and 16 are consistent.

4.4. Capture efficiency and pressure drop of dust-loaded fibers

The growth of dendrites results in the expansion of capture range and the increase of pressure drop and capture efficiency of fibers.

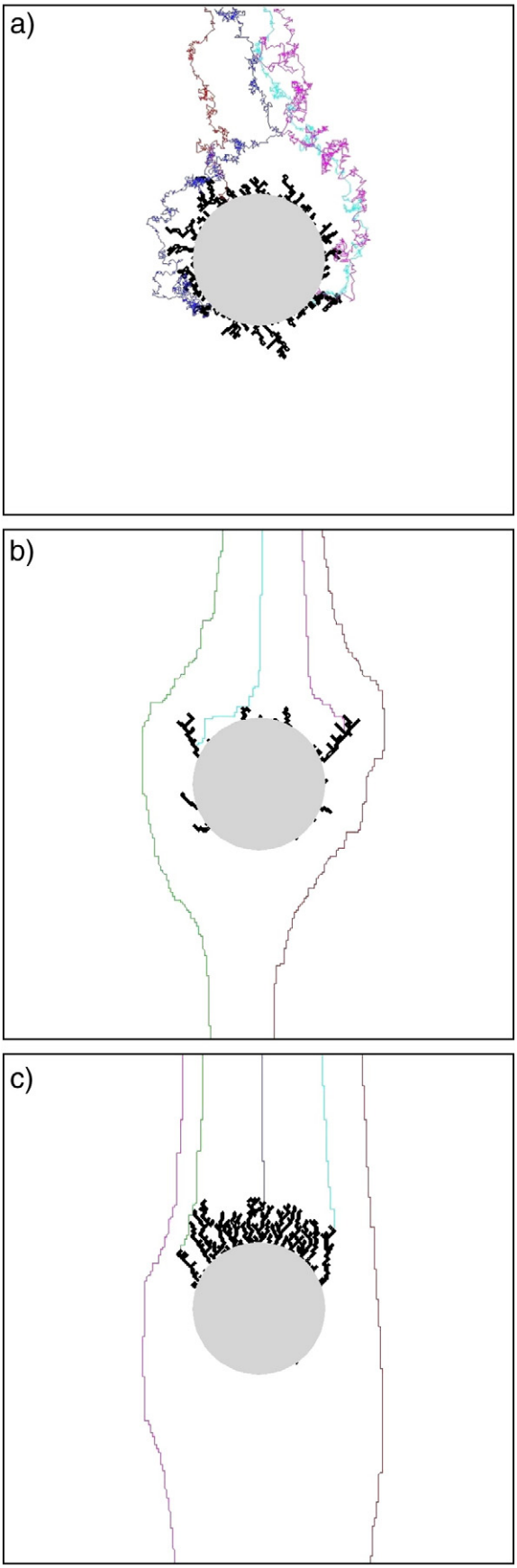

Fig. 13. Typical particle trajectories during the clogging processes: (a) predominant Brownian diffusion; (b) predominant interception; (c) predominantly inertial impaction.

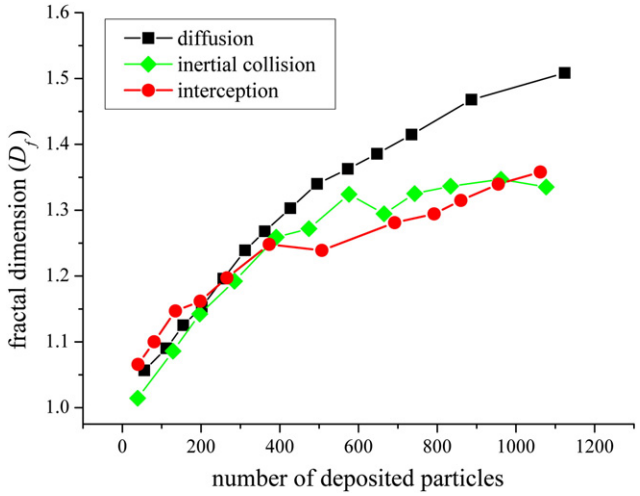

Fig. 14. Fractal dimension vs the number of deposited particles during the clogging processes.

Kasper et al. [50] obtained a formula through experiments to characterize the raising of capture efficiency and the mass of loaded particles. In our simulation, the following parameters are chosen: $St = 0.3$, $d_p = 1.3$ μm, $d_f = 30$ μm, $\rho_p/\rho_f = 764.3$. Our simulation results agree well with the model predictions of Kasper et al. (see Fig. 17), which further validates the ability of the LB–CA model for the filtration processes of not only clean fibers but also dust-loaded fibers.

There is an empirical model for pressure drop of dust-loaded fibers [51–53]:

$$\begin{cases} \Delta P = 64\mu U d \dfrac{\left(\alpha'\right)^{3/2}\left[1+56\left(\alpha'\right)^3\right]}{d_f^2} \\ \alpha' = K_d^2\alpha; d'_f = K_d d_f; K_d = 1 + W_d/\left(\alpha\rho_p h\right) \end{cases} \tag{22}$$

where K_d is the dust-loaded coefficient, W_d is the loaded mass of unit area. The dimensionless drag force can be defined as: $F^*/F_0{}^* = \Delta P/\Delta P_0$, where ΔP_0 is the pressure drop of a clean fiber. Fig. 18 presents the dynamic evolution of pressure drop during the clogging process. It looks the empirical model overpredicts the pressure drop when the loaded mass is increasing.

5. Conclusions

The Lattice Boltzmann-cell automation model offers a useful tool for description of the gas–solid flows, where gas dynamics is solved

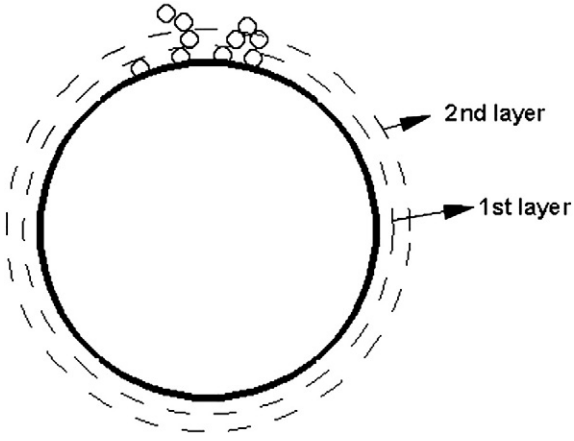

Fig. 15. Schema of deposition layers.

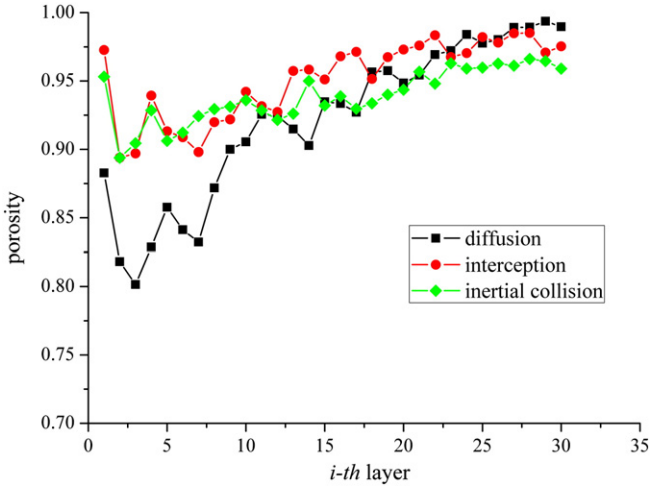

Fig. 16. Porosity distribution in thickness direction.

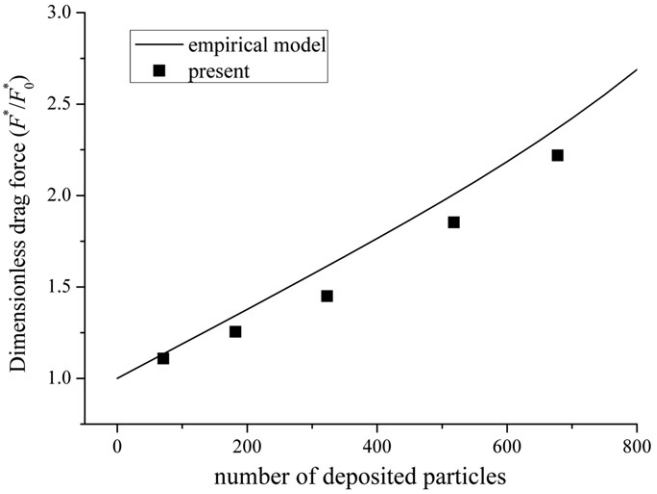

Fig. 18. Pressure drop of dust-load fiber.

by the LB method while the solid particle motion is described by the CA probabilistic approach. Different from the traditional LB-Lagrangian model, solid particles in the lattice Boltzmann-cellular automation model are constrained to only move on the same regular lattices as the fluid particles, and their transport probabilities to neighboring nodes depend on the local fluid flow and other external forces subject to solid particles. In the Lattice Boltzmann-cellular automation model, the interaction between gas–solid flow and complex and unsteady geometric boundary can be easily realized. However, the existing Lattice Boltzmann-cellular automation model is able to describe particle behaviors only on the level of qualitative simulation because some empirical or tentative formulations/parameters are introduced so that the effect of fluid on particle transport is roughly estimated. In this paper, the Lattice Boltzmann-cellular automation model is for the first time improved to describe particle transport under consideration of combined effects such as Brownian diffusion, drag force, and other external forces. The actual displacement of a particle within a time step is accurately calculated from the Lagrangian equations of motion for a particle, in such a way that the transport probabilities of a solid particle to neighboring nodes is determined by the ratio of its actual displacement on a lattice direction and the lattice length of the direction.

The Lattice Boltzmann-cellular automation model is used to describe the steady and unsteady filtration process, including the steady capture efficiency and pressure drop during the filtration processes of clean fibers, the dynamic evolution of the branch cluster structure, capture efficiency and pressure drop along with particle loading. Our results are in good agreement with previous theoretical predictions and experimental observations. The Lattice Boltzmann-cellular automation model presented in this paper is able to quantitatively describe the filtration process, owing to correct consideration of fluid–particle interaction. The filtration processes of clean fibers or dust-loaded fibers are simulated when only one capture mechanism (Brownian diffusion, interception, or inertial impaction) predominates (although the three capture mechanisms have either strong or weak effects on the filtration processes in our simulation). The detailed information on the particle trajectories and the dendrite structures are obtained. An isotropic distribution of particles around the fiber with relatively open pore structure is formed for the diffusion-controlled deposition; when interception mechanism dominates, the structure of dendrites becomes more branched and open; particles with larger inertia collide with the windward of fibers, resulting in a dendrite with compact structure (steady fractal dimension and lower porosity).

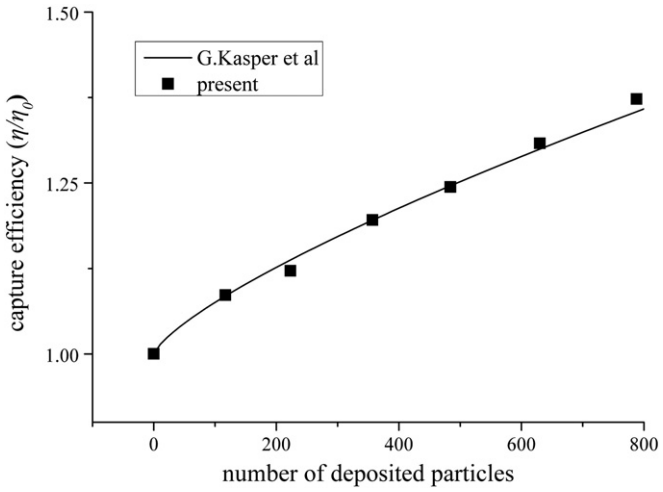

Fig. 17. Capture efficiency vs loaded particles number.

This paper only considered the filtration process of single fiber or a row of cylindrical fibers in a laminar flow normal to their axes. These cases can be viewed to be two-dimensional gas–solid flows. The reliable predictions will help construct the optimal fibrous filter structures, and provide basic model parameters and constitutive equations for macroscopic modeling of penetration and press drop. However, it should be mentioned that in the real case of fibrous assembly, in addition to single fiber theory, size and shape of pores defined by the fibrous assembly as well the orientation of fibers play a vital role in particle filtration. Capturing by filter media can also be distinguished as surface and depth filtration. As for these real cases, three-dimensional simulation should be considered. The Lattice-Boltzmann gas–solid flow model is able to deal with complex and dynamic boundary conditions, and is thus a promising candidate for numerical simulation of particle filtration by real fibrous assembly.

Acknowledgments

The authors were supported by “the National Natural Science Foundation of China under grant numbers 50876037 and 51021065”, and “Program for New Century Excellent Talents in University” (NCET-10-0395), “National Key Basic Research and Development Program” (2010CB227004), and “State Key Laboratory of Multiphase Complex Systems”(MPCS-2011-D-02).

Reference

[1] C. Tien, C.S. Wang, D. Barot, Chainlike formation of particle deposits in fluid–particle separation, Science 196 (4293) (1977) 983.
[2] S. Friedlander, Mass and heat transfer to single spheres and cylinders at low Reynolds numbers, AIChE Journal 3 (1) (1957) 43–48.

[3] K. Lee, B. Liu, Experimental study of aerosol filtration by fibrous filters, Aerosol Science and Technology 1 (1) (1981) 35–46.
[4] T. Myojo, C. Kanaoka, H. Emi, Experimental observation of collection efficiency of a dust-loaded fiber, Journal of Aerosol Science 15 (4) (1984) 483–489.
[5] D. Japuntich, J. Stenhouse, B. Liu, Experimental results of solid monodisperse particle clogging of fibrous filters, Journal of Aerosol Science 25 (2) (1994) 385–393.
[6] S. Dunnett, C. Clement, A numerical study of the effects of loading from diffusive deposition on the efficiency of fibrous filters, Journal of Aerosol Science 37 (9) (2006) 1116–1139.
[7] C. Zhu, C.H. Lin, C.S. Cheung, Inertial impaction-dominated fibrous filtration with rectangular or cylindrical fibers, Powder Technology 112 (1–2) (2000) 149–162.
[8] Z.G. Liu, P.K. Wang, Pressure drop and interception efficiency of multifiber filters, Aerosol Science and Technology 26 (4) (1997) 313–325.
[9] Q. Wang, B. Maze, H. Tafreshi, A case study of simulating submicron aerosol filtration via lightweight spun-bonded filter media, Chemical Engineering Science 61 (15) (2006) 4871–4883.
[10] B. Maze, H. Tafreshi, Q. Wang, A simulation of unsteady-state filtration via nanofiber media at reduced operating pressures, Journal of Aerosol Science 38 (5) (2007) 550–571.
[11] S. Hosseini, H. Tafreshi, Modeling particle filtration in disordered 2-D domains: a comparison with cell models, Separation and Purification Technology 74 (2) (2010) 160–169.
[12] A. Dupuis, B. Chopard, Lattice gas modeling of scour formation under submarine pipelines, Journal of Computational Physics 178 (2002) 161–174.
[13] M.D. Mazzeo, P.V. Coveney, HemeLB: a high performance parallel lattice-Boltzmann code for large scale fluid flow in complex geometries, Computer Physics Communications 178 (12) (2008) 894–914.
[14] C.K. Aidun, J.R. Clausen, Lattice-Boltzmann method for complex flows, Annual Review of Fluid Mechanics 42 (2010) 439–472.
[15] A. Ladd, R. Verberg, Lattice-Boltzmann simulations of particle–fluid suspensions, Journal of Statistical Physics 104 (5) (2001) 1191–1251.
[16] A. Ladd, Short-time motion of colloidal particles: numerical simulation via a fluctuating lattice-Boltzmann equation, Physical Review Letters 70 (9) (1993) 1339–1342.
[17] S. Balachandar, J.K. Eaton, Turbulent dispersed multiphase flow, Annual Review of Fluid Mechanics 42 (2010) 111–133.
[18] O. Filippova, D. Hänel, Lattice-Boltzmann simulation of gas-particle flow in filters, Computers & Fluids 26 (7) (1997) 697–712.
[19] U. Lantermann, D. Hänel, Particle Monte Carlo and lattice-Boltzmann methods for simulations of gas-particle flows, Computers & Fluids 36 (2) (2007) 407–422.
[20] M. Chopard, A lattice Boltzmann model for particle transport and deposition, Europhysics Letters 42 (3) (1998) 259–264.
[21] B. Chopard, A. Masselot, Cellular automata and lattice Boltzmann methods: a new approach to computational fluid dynamics and particle transport, Future Generation Computer Systems 16 (2–3) (1999) 249–257.
[22] B. Chopard, A. Masselot, A. Dupuis, A lattice gas model for erosion and particles transport in a fluid, Computer Physics Communications 129 (2000) 167–176.
[23] B. Chopard, M. Droz, Cellular Automata Modeling of Physical Systems, Cambridge University Press, Cambridge, UK, 1998.
[24] U. Frisch, B. Hasslacher, Y. Pomeau, Lattice-gas automata for the Navier–Stokes equation, Physical Review Letters 56 (14) (1986) 1505–1508.
[25] R. Przekop, A. Moskal, L. Gradoń, Lattice-Boltzmann approach for description of the structure of deposited particulate matter in fibrous filters, Journal of Aerosol Science 34 (2003) 133–147.
[26] R. Przekop, L. Gradoń, Deposition and filtration of nanoparticles in the composites of nano- and microsized fibers, Aerosol Science and Technology 42 (2008) 483–493.
[27] Y.H. Qian, D. d'Humieres, P. Lallemand, Lattice BGK models for Navier–Stokes equation, Europhysics Letters 17 (1992) 479.
[28] S. Chen, Z. Wang, X. Shan, Lattice Boltzmann computational fluid dynamics in three dimensions, Journal of Statistical Physics 68 (3) (1992) 379–400.
[29] P. Bhatnager, E. Gross, M. Krook, A model for collision process in gases, Physical Review 94 (1954) 511.
[30] T. Abe, Derivation of the lattice Boltzmann method by means of the discrete ordinate method for the Boltzmann equation, Journal of Computational Physics 131 (1) (1997).
[31] Z. Guo, C. Zheng, B. Shi, Discrete lattice effects on the forcing term in the lattice Boltzmann method, Physical Review E — Statistical, Nonlinear, and Soft Matter Physics 65 (4 Pt 2B) (2002) 046308.
[32] S. Hou, J. Sterling, S. Chen, et al., A lattice Boltzmann subgrid model for high Reynolds number flows, Pattern formation and lattice gas automata, 6, 1996, p. 149.
[33] B. Chopard, L. Frachebourg, M. Droz, Multiparticle lattice gas automata for reaction diffusion systems, International Journal of Modern Physics C-Physics and Computer 5 (1) (1994) 47–64.
[34] J. Wei, F.E. Kruis, Simulation of particle diffusion and convection in finite volume cells via a random walk method, 6th International Conference on Multiphase Flow, 2007, Leipzig, Germany.
[35] H.N. Unni, C. Yang, Brownian dynamics simulation and experimental study of colloidal particle deposition in a microchannel flow, Journal of Colloid and Interface Science 291 (2005) 28–36.
[36] M. Kim, A. Zydney, Effect of electrostatic, hydrodynamic, and Brownian forces on particle trajectories and sieving in normal flow filtration, Journal of Colloid and Interface Science 269 (2) (2004) 425–431.
[37] R. Maniero, P. Canu, A model of fine particles deposition on smooth surfaces: I—theoretical basis and model development, Chemical Engineering Science 61 (2006) 7626–7635.
[38] A. Li, G. Ahmadi, Dispersion and deposition of spherical particles from point sources in a turbulent channel flow, Aerosol Science and Technology 16 (4) (1992) 209–226.
[39] Z. Guo, C. Zheng, B. Shi, Non-equilibrium extrapolation method for velocity and pressure boundary conditions in the lattice Boltzmann method, Chinese Physics 11 (2002) 366.
[40] Z. Guo, T.S. Zhao, Explicit finite-difference lattice Boltzmann method for curvilinear coordinates, Physical Review E — Statistical, Nonlinear, and Soft Matter Physics 67 (6) (2003) 066709.
[41] S.M. Greenfield, Rain scavenging of radioactive particulate matter from the atmosphere, Journal of Atmospheric Sciences 14 (1957) 115–125.
[42] I. Stechkina, N. Fuchs, Studies on fibrous aerosol filters—I. Calculation of diffusional deposition of aerosols in fibrous filters, Annals of Occupational Hygiene 9 (2) (1966) 59.
[43] H.C. Yeh, B.Y.H. Liu, Aerosol filtration by fibrous filters—I. theoretical, Journal of Aerosol Science 5 (2) (1974) 191–204.
[44] R.C. Brown, Air Filtration: An Integrated Approach to the Theory and Applications of Fibrous Filters, Pergamon Press, 1993.
[45] K.W. Lee, B.Y.H. Liu, Theoretical study of aerosol filtration by fibrous filters, Aerosol Science and Technology 1 (2) (1982) 147–161.
[46] K.W. Lee, J.A. Gieseke, Note on the approximation of interceptional collection efficiencies, Journal of Aerosol Science 11 (4) (1980) 335–341.
[47] T. MIYAGI, Viscous flow at low Reynolds numbers past an infinite row of equal circular cylinders, Journal Of the Physical Society of Japan 13 (5) (1958).
[48] C. Kanaoka, H. Emi, T. Myojo, Simulation of the growing process of a particle dendrite and evaluation of a single fiber collection efficiency with dust load, Journal of Aerosol Science 11 (4) (1980) 377–383.
[49] G. Kasper, S. Schollmeier, J. Meyer, Structure and density of deposits formed on filter fibers by inertial particle deposition and bounce, Journal of Aerosol Science 41 (12) (2010).
[50] G. Kasper, S. Schollmeier, J. Meyer, The collection efficiency of a particle-loaded single filter fiber, Journal of Aerosol Science 40 (12) (2009) 993–1009.
[51] D. Thomas, P. Penicot, P. Contal, Clogging of fibrous filters by solid aerosol particles experimental and modelling study, Chemical Engineering Science 56 (11) (2001) 3549–3561.
[52] D. Thomas, P. Contal, V. Renaudin, Modelling pressure drop in HEPA filters during dynamic filtration, Journal of Aerosol Science 30 (2) (1999) 235–246.
[53] W. Bergman, R. Taylor, H. Miller, Enhanced filtration program at LLNL, 15th DOE Nuclear Air Cleaning Cong, Boston, 1978.